Polydiapirs: multiwavelength gravity structures

ROBERTO FERREZ WEINBERG and HARRO SCHMELING*

Hans Ramberg Tectonic Laboratory, Institute of Geology, University of Uppsala, Box 555, S-751 22,
Uppsala, Sweden

Abstract—Polydiapirs (domes-in-domes) result from the evolution of a multiwavelength Rayleigh–Taylor (gravitational) instability. The present work investigates the initiation and development of polydiapirs by means of two-dimensional finite-difference models of gravitationally unstable triple-layered sequences of Newtonian fluids. The values of viscosities, thicknesses and densities were systematically varied for selected examples. In triple-layered sequences, only two types of density stratification are likely to result in multiwavelength instabilities that will eventually develop into polydiapiric structures. The limiting factors and evolution of such structures were studied for both these types of density stratifications.

Finite-difference calculations on models with physical parameters appropriate to evaporitic sequences and covered by a viscous clastic overburden showed that a very small downward density decrease in the evaporitic source may cause an internal overturn that will compete with the main overturn between source and overburden. This may lead to the development of sequential or simultaneous polydiapirs. The mature polydiapirs in the models exhibit spines, curtain folds, pendant repetitions of the source layers inside the large diapirs, and anomalous interdiapiric distances. All these features are known in natural salt diapirs suggesting that polydiapirs may be far more common in nature than hitherto recognized.

INTRODUCTION

POLYDIAPIRS, the structures resulting from a multiwavelength Rayleigh–Taylor instability, have been proposed as an explanation for complex structures observed in Pre-Cambrian terrains (e.g. Stephansson 1975, Schwerdtner 1982, Collins 1989). However, the conditions for the development of such structures and their geometry at mature stages are unknown. The present paper describes systematic experiments exploring the evolution of polydiapirs.

Diapir is the non-genetic geological term applied to ductile intrusive structures. Many diapirs may develop due to the rise of gravitationally unstable buoyant fluids through denser overburden. Such gravitationally unstable configurations consisting of viscous layers are known as Rayleigh–Taylor instabilities. The spacing and geometry of diapiric structures have been extensively studied in nature (e.g. Jackson *et al.* 1990), and in physical and numerical experiments (e.g. Ramberg 1968, 1981, Woidt 1978, Schmeling 1987, Jackson *et al.* 1988, 1990).

Biot & Odé (1965) argued that, given random perturbation at the interface between a buoyant layer and a denser viscous overburden, the instability will develop a characteristic wavelength, λ_c, which grows at a faster rate than any other wavelength and dominates the mature stages of the gravity overturn. The λ_c of gravity-driven diapirs is controlled mainly by the thickness and viscosity contrasts between the buoyant source layer and its denser overburden. The density differences between the two layers control primarily the rate of overturn (Ramberg 1981).

Applying linear stability analysis, Ramberg (1968, 1973) was the first to draw attention to the possibility that two different characteristic wavelengths could develop simultaneously in a model with two buoyant source layers covered by a denser overburden. The resulting multiwavelength structure was termed 'domes-in-domes' (Ramberg 1973), or polydiapirs (Stephansson 1975); the latter term is adopted here. Polydiapirism has been proposed to explain the structural pattern of the Early Proterozoic batholiths of the Baltic Shield (Stephansson 1975). The occurrence of similar structures has been proposed in Archaean terrains in the Superior Province of Canada (Schwerdtner 1982), and in the Mount Edgar Batholith of Western Australia (Collins 1989). According to the latter four authors, polydiapiric structures developed from triple-layered rock sequences with inverse density stratification.

Ramberg's (1968, 1973) linear stability analysis was limited to the very early stages of diapirism in triple layers (amplitudes <10% of the wavelength). Polydiapirs caused by the imposition of small parasitic diapirs in double-layered sequences with long characteristic wavelength were systematically studied by Schmeling (1987). Jackson *et al.* (1988) and Jackson & Talbot (1989b) also produced polydiapirs in downbuilding centrifuged models where the smaller initially formed diapirs became incorporated into larger ones as the characteristic wavelength increased during thickening of the overburden. The present paper describes systematic experiments showing the evolution of polydiapirism in three viscous layers.

Triple-layered sequences may have six types of density stratification (Fig. 2), but only three of these may develop polydiapirs. The ratios of viscosities, densities and thicknesses that control the wavelength and the growth rate of the instabilities were systematically

---

*Present address: University of Bayreuth, Bayerisches Geoinstitut Postfach 102051, D-8580 Bayreuth, Germany.

varied to explore the way in which each influences the development of polydiapirs. A physical model was constructed to explore the effects of the third dimension. A final discussion compares the results of models to natural examples of internal structures observed in salt diapirs.

THE METHOD

Model design and limitations

The initial geometry and physical parameters of the models used for calculations are shown in Fig. 1. All layers have constant Newtonian viscosity, and the viscosities of the two lower layers were kept equal in all calculation series. The perturbation grows from white noise, such that the fastest growing wavelength dominates at finite strains as a characteristic wavelength. The box had boundary conditions characterized by no-slip at the bottom, free-slip at the top, and reflective lateral boundaries. Both 58 × 38 grid intersections and 160 × 110 markers were used in the calculations. In order to avoid the influence of the lateral boundaries on the wavelength developed in the model, the box should be of an infinite length. However, as the length of the box is increased, the resolution of the calculations is decreased due to decreased density of the markers. The length of the box was therefore chosen to be approximately the same size as the characteristic wavelength calculated from linear stability analysis. The influence of box length on the structures was checked in a few runs where only this parameter was varied. The effect of these variations is to change the form of the random perturbation, and allow the development of wavelengths which are slightly different from the characteristic one. However, the results show that similar structures develop for box sizes up to 20% longer than the characteristic wavelength.

Newtonian fluids were modelled because they simplify the calculations and interpretation of the results. However, in nature only salt is likely to show Newtonian behaviour (Urai et al. 1986). Other sedimentary and igneous rocks probably behave as non-Newtonian fluids

or as brittle solids, depending on such factors as their depth of burial, temperature, etc. Yield strength and non-Newtonian behaviour of the materials involved in the unstable sequence would cause significant changes in the growth rate and in the time of initiation of the instabilities. Faults in the overburden layer in regions of salt diapirism (e.g. Jenyon 1986), demonstrate brittle behaviour that will greatly affect the evolution of the diapirs. Rayleigh–Taylor instabilities are not a good analogue for this type of behaviour. However, since evaporitic layers do behave as fluids, the internal structures of the diapirs caused by internal flow during rise or by any internal density inversion will still occur and many of the internal polydiapiric structures shown here will still develop.

Mathematical formulation

The dynamics of fluid flow driven by compositionally induced density variations (e.g. diapirism developed from Rayleigh–Taylor instabilities) can be described by the equations of conservation of mass, momentum and composition. Neglecting inertial forces and assuming incompressibility, these equations are given as, respectively,

$$\frac{\partial \rho}{\partial t} + \nabla(\rho \mathbf{v}) = 0 \qquad (1)$$

$$0 = -\nabla P + \frac{\partial \tau_{ji}}{\partial x_j} + \rho \mathbf{g} \qquad (2)$$

$$0 = \frac{\partial c_k}{\partial t} + \mathbf{v}\nabla c_k, \qquad (3)$$

where $\mathbf{v}$ is the flow velocity, P the pressure, τ_{ij} the deviatoric stress tensor, ρ the density, $\mathbf{g}$ the gravity acceleration, t the time, and c_k the concentration of the k-th chemical component. At any location, the concentrations of the different components add up to 1, i.e.

$$\sum_{k=1}^{n_{mat}} c_k = 1 \qquad (4)$$

if n_{mat} is the number of components of the problem.

This definition allows consideration of chemical mixtures of different materials (different c_ks are >0 at the same location) as well as immiscible fluids (the c_k is equal to 1 only at the positions which are occupied by the material k, otherwise it is 0).

The stress in equation (2) can be expressed in terms of the velocities by using the constitutive law

$$\tau_{ij} = 2\eta_k \dot{e}_{ij}, \qquad (5)$$

where η_k is the viscosity of the k-th component and $\dot{e}_{ij}$ is the strain-rate tensor, defined as

$$\dot{e}_{ij} = \tfrac{1}{2}\left(\frac{\partial v_i}{\partial x_j} + \frac{\partial v_j}{\partial x_i}\right). \qquad (6)$$

At boundaries between different materials, mixing might occur due to numerical diffusion. An effective
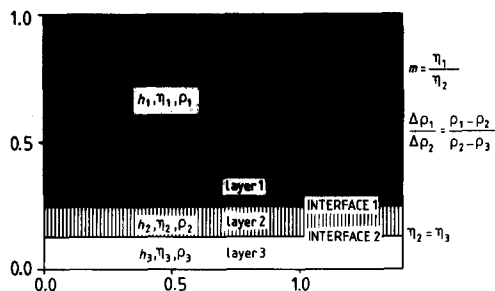
Fig. 1. Box showing the initial geometrical conditions and the non-dimensional physical variables used in the calculations. No initial perturbation is imposed; the perturbations grow from white noise. The box has no-slip at the bottom, free-slip at the top and reflective side boundaries. The length of the box can be varied and the initial amplitude of the white noise is 0.24% of the box height. The horizontal and vertical axes are scaled by the height of the box.

viscosity has to be defined for these regions. Assuming that in mixtures of different compositions the total strain rate is given as the sum of the strain rates in each component (assuming the same stress), the effective viscosity of a mixture can be defined as

$$\eta = \left(\sum_k \frac{c_k}{\eta_k} \right)^{-1}. \tag{7}$$

To specify the density in the buoyancy term of equation (2) we take the mean of the densities of the different materials weighted by their concentrations

$$\rho = \sum_k c_k \rho_k. \tag{8}$$

From (8) it is clear that in any pure region k, the density is equal to ρ_k.

Multiplying equation (3) with ρ_k, summing them over all k and inserting the density according to (8) gives

$$\frac{\partial \rho}{\partial t} + \mathbf{v} \nabla \rho = 0. \tag{9}$$

Inserting this into the continuity equation (1) we obtain

$$\nabla \mathbf{v} = 0. \tag{10}$$

Thus, we can introduce the stream-function ψ as

$$\mathbf{v} = \begin{pmatrix} \dfrac{\partial \psi}{\partial z} \\ -\dfrac{\partial \psi}{\partial x} \end{pmatrix} \tag{11}$$

which automatically fulfils the continuity condition (10). Using the constitutive law (5) with (6) and using the stream-function from (11) we can eliminate the deviatoric stresses in (2). Assuming two-dimensionality, we can take the curl of equation (2), which eliminates the pressure. The equation of motion (2) is then given as

$$4\frac{\partial^2}{\partial x \partial z} \eta \frac{\partial^2 \psi}{\partial x \partial z} + \left(\frac{\partial^2}{\partial z^2} - \frac{\partial^2}{\partial x^2} \right) \eta \left(\frac{\partial^2 \psi}{\partial z^2} - \frac{\partial^2 \psi}{\partial x^2} \right)$$
$$= -\mathbf{g} \sum_k \rho_k \frac{\partial c_k}{\partial x}, \tag{12}$$

where x and z are the horizontal and vertical coordinates, respectively. Given the chemical concentrations $c_k(x,z,t)$, the biharmonic equation (12) can be solved numerically.

For the conservation of composition, the field equation (3) is not solved directly; instead a marker approach is used. Following any fluid particle on its flow path, equation (3) may be written in the Lagrangian reference system

$$\left(\frac{\partial c_k}{\partial t} \right)_{\text{particle}} = 0. \tag{13}$$

Thus, equation (13) implies that we have to solve for the flow path equation

$$\left(\frac{\partial \mathbf{x}}{\partial t} \right)_{\text{particle}} = \mathbf{v} \tag{14}$$

and have to ensure that the c_k values remain constant at $x(t)_{\text{particle}}$.

Numerical solutions

The biharmonic equation (12) is solved by finite differences in a rectangular region on an equidistant grid. Cholesky decomposition of the symmetric matrix determined from the biharmonic operator is used. To solve (14) the region is filled with closely spaced marker points (approximately 10–50 markers per finite difference cell). Each marker is assigned its particular chemical composition, i.e. $c_k(x_m)$, where $x_m(t)$ is the position of a marker at the time t. Equation (14) is then solved for all markers by a combination of fourth-order Runge–Kutta integration with a predictor–corrector step.

For the solution of (12), the c_k-values have to be known at the finite difference grid points at each time step. This is accomplished by simply taking the average values of all markers, which are found within half of a grid distance from the specific grid point. A weighted average does not significantly improve the accuracy, but is considerably more time consuming.

An advantage of the marker approach is that it introduces no numerical diffusion. This would have been a significant problem if the field equation (3) had been solved directly. However, large deformation during the flow history and small numerical fluctuation of the marker positions (they may jump from their flow paths due to the finite resolution of the velocity field) may lead to situations in which no markers are found within a half grid spacing of one grid point prohibiting the updating of the c-field mentioned above. In this case, a new marker field has to be created from weighted interpolation of the old one. During such repartitioning of the marker field, numerical diffusion will be introduced with a maximum diffusion length of one finite difference grid space. Depending on the number of markers, such repartitioning steps have to be done after several tens to a few hundred time steps.

The markers are initially distributed on a rectangular (marker) grid with small random displacements. These fluctuations, which have a maximum amplitude of a half marker grid distance, are also responsible for the initial perturbations of the horizontal interfaces between materials of different density (in the form of white noise). The effective amplitude of the white noise perturbation is 0.24% of the total box thickness for a 200 × 200 marker grid.

The accuracy of the method has been checked in different ways. The conservation of chemical composition is controlled during runs by taking the global average of all compositions, and by integrating over particular c_k-components. During one Rayleigh–Taylor overturn, relative changes in total compositions are less than 0.1%, for the finite difference grids of 81 × 46 and 300 × 300 markers used in the models.

Several runs tested the algorithm. Rayleigh–Taylor instabilities with different viscosity contrasts have been modelled, and compared with growth rates known from analytical solutions (e.g. Ramberg 1981). A crude finite difference grid of only 46 × 31 nodes and 150 × 150 markers reproduces the analytical growth rates with an accuracy over 2%. These tests have been carried out with viscosity contrasts up to 1000. It is noteworthy that the finite difference form of the biharmonic operator in equation (12) is able to handle such large viscosity contrasts correctly.

RESULTS

This section starts with a brief outline of the results to aid the presentation of the details. All numerical models calculated in this study are composed of three layers, numbered 1–3 from top to bottom; each interface was assigned the number of its overlying layer. Triple-layered sequences may present six different density stratifications (Fig. 2). Case I is gravitationally stable, and cases II and III will always develop a single wavelength. Multiwavelength instabilities only develop in cases IV, V and VI.

Density stratifications like those of case IV (Fig. 2) may develop multiwavelength only if the top layer (1) is sufficiently stiff relative to the two underlying layers. In this case, the overturn occurs sequentially in two steps. The first step is a short wavelength overturn between layers 2 and 3 before the upper layer is involved; interface 1 acts as an almost rigid boundary. The second step occurs when diapirs of layer 3, after accumulating below layer 1, eventually rise through this layer. The controls on the wavelength at each of the two steps are different and may lead to different wavelengths. This type of evolution, in which different wavelengths develop at different stages, is distinguished here as 'sequential polydiapirism'.
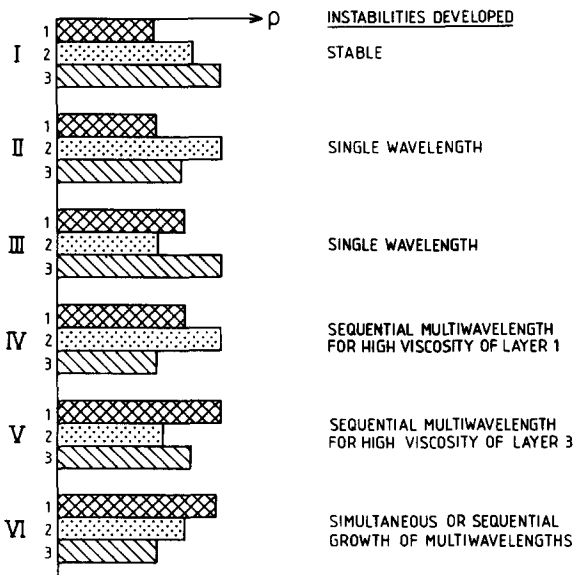

Fig. 2. The six possible types of density stratification in triple-layered sequences.

The same rationale can be used for case V. A two-stage evolution may occur if layer 3 is stiffer than the overlying layers. Layers 1 and 2 overturn in short wavelength diapirs before a later overturn between layers 1 and 3 occurs on a larger wavelength. However, results of model calculations show that even when layer 3 is very stiff ($\eta_3 = 1000\,\eta_2$) it will be sucked up beneath diapirs of the less dense layer 2. This results in a single wavelength overturn. Although polydiapirs may occur if layer 3 is even more viscous, case V density stratification is not considered further here because of the numerical problems in the computer program caused by viscosity contrasts $>10^3$.

Simultaneous growth of multiwavelength diapirs is only likely in density stratification case VI. This case presents two gravitationally unstable layers that will actively overturn. If the characteristic wavelengths of the two interfaces are similar only one set of diapirs develops. But if the wavelengths of the two overturns differ significantly, both will develop, simultaneously if their growth rates are similar, or sequentially if their growth rates are different.

A series of calculations investigated models with density stratifications of cases IV and VI, where thickness (h), density (ρ) and viscosity (η), of all the three layers was systematically varied. Case VI was studied in greater detail because the simultaneous and sequential polydiapirs developed a series of structures relevant to natural salt diapirs, including spines, curtain folds, repetition of layers inside the diapir, and anomalous interdiapiric spacing.

Case IV: single source, a mobile lower overburden and a stiff upper overburden

The density stratification of case IV corresponds to a natural sedimentary sequence where a layer of rock salt is covered by dense and mobile anhydrite, which in turn is overlain by stiff sedimentary rocks with density lower than anhydrite (e.g. Sverdrup Basin, Canada; Schwerdtner & Osadetz 1983). A similar situation can be visualized for a granitic magma underlying a dense, warm and mobile lower crust, overlain by a less dense and stiffer middle crust. A series of two-dimensional finite difference models were calculated where the viscosities of the two lower layers were assumed to be equal, and the viscosity ratio (m), between the upper and middle layers was varied. The thicknesses were also varied.

Three calculations were made simulating evaporites where only the parameter m was varied (Fig. 3). The results show that for increasing values of m, the structures developed change from single wavelengths to sequential polydiapirs. The structures developed where $m = 2$ (Fig. 3a) show a single wavelength and the overturn was not influenced by the slightly stiffer upper layer. Mushroom-shaped diapirs form at the third step (Fig. 3a), as predicted by Jackson & Talbot (1986), for layers with the same viscosity (layers 2 and 3). Mushroom shapes tend to develop into finger shapes as diapirs
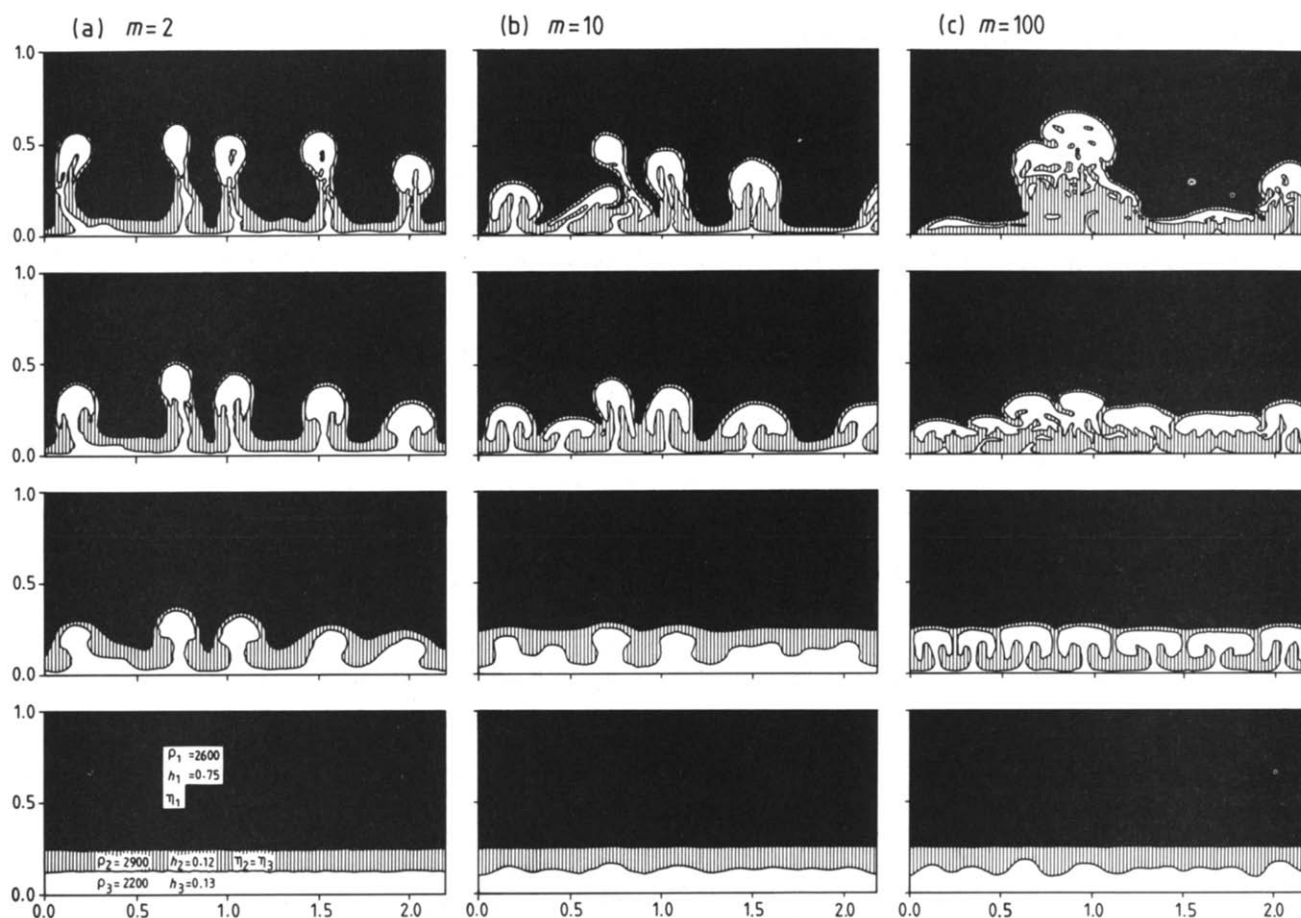
Fig. 3. Results of calculations in models with the density stratifications of case IV where only the viscosity ratio (m) between layers 1 and 2–3 was varied. The physical and geometrical parameters for all models are specified in the lower left diagram, densities are in kg cm^{-3}. In all models the denser layer 2 (e.g. anhydrite) was entrained by the rising diapirs of layer 3 in the form of internally isolated blocks or tails.

penetrate the more viscous overburden layer 1 (fourth step in Fig. 3a). Comparing the results obtained with the graphs in Rönnlund (1989), it may be concluded that the wavelength is approximately controlled by the thickness ratio between the source and the whole overburden, and by the viscosity contrast between the source and overburden 2. Minor variations in the viscosity of layer 1 may cause variation in λ_c.

When $m = 100$ (Fig. 3c) the stiff layer acts as a rigid boundary, causing spreading and accumulation of the short-wavelength diapirs beneath it. The wavelength of this first phase of overturn is controlled only by the parameters of the two layers involved, i.e. the viscosity ratio and the relative thickness of source layer 3 and layer 2. As these small diapirs accumulate beneath layer 1, they deform interface 1 causing a new overturn on a longer wavelength. The factors now controlling the new wavelength are the relative thickness of the source (layer 3) and layer 1, and their relative viscosity. At this point layer 2 is under layer 3 and acts as a low viscosity dense basement as the new wavelength develops. As a result of the first overturn, the thickness of the source is highly variable, and entrained inclusions of the original overburden layer 2 will rise together with the diapirs. The final result is a complex structure where the small diapirs of the first overturn merge to form the large diapirs required by the new and longer wavelength of the

second overturn. If the viscosity contrast was significantly higher than 100, the first overturn between source and overburden would be complete before the second; the initial layer 3 would swap places with layer 2 before the initiation of the second overturn. The later overturn would then be accomplished without any signs of the first overturn and polydiapirism would not occur.

The calculations made for $m = 10$ (Fig. 3b) show an intermediate situation between the two extremes described above. Some of the small diapirs show a tendency to coalesce and try to form larger diapirs and others develop independently.

The models presented above assume layers 2 and 3 to have the same viscosity. However geological evidence shows that anhydrite is less mobile than halite (Richter-Bernburg 1980). A model was therefore calculated where layer 2 was more viscous than layer 3. The following dimensional viscosities given in Pa s were assigned for the three layers: $\eta_1 = 10^{20}$, $\eta_2 = 5 \times 10^{18}$ and $\eta_3 = 5 \times 10^{17}$. The result was the development of polydiapirs in a sequential multiwavelength overturn similar to that shown in Fig. 3(c).

Comparison of the results in Fig. 3 allows a definition of the factors limiting the development of polydiapirism. The viscosity contrast between the upper and lower overburdens has to be sufficiently high for the upper overburden to act initially as an effectively rigid bound-
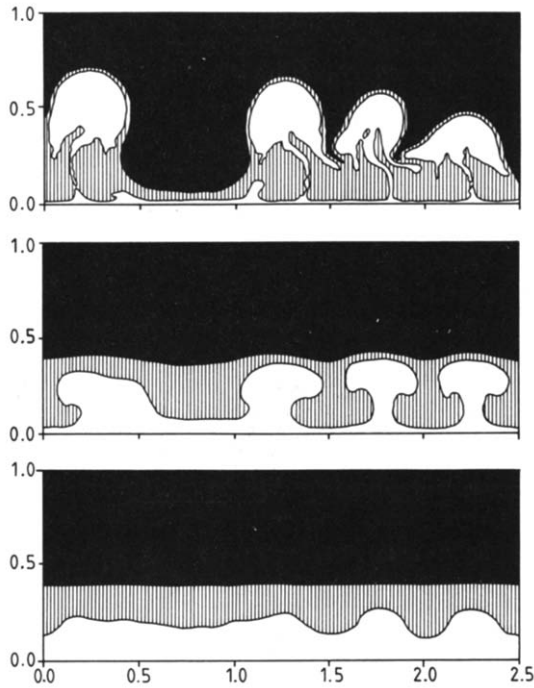
Fig. 4. Structures developed in a calculation of case IV with parameters similar to Fig. 3, where $m = 20$ and an initial thickness of the two lower layers of 0.4 of the box height.

ary beneath which diapirs of the first overturn accumulate before the subsequent overturn occurs on a larger scale. For the model parameters above, $m = 10$ represents the transition between cases of simple diapirs and polydiapirs. When the upper layer acts as an effective rigid boundary during the first overturn, the model simplifies to a simple two-layer case where layer 1 may be disregarded. The λ_c can then be calculated by Woidt's equations (1980) and Rönnlund's graphs (1989) for no-slip at both top and bottom boundaries.

Were the combined thicknesses of layers 2 and 3 to be increased in relation to the thickness of layer 1, the wavelength of the first overturn would increase and its influence on interface 1 would be stronger due to the larger volumes involved in the overturn. Eventually this influence might be so strong that layer 1 would deform early in the development of the instability, and the wavelength of the first overturn dominates (Fig. 4).

The main effect of density variations between the three layers is to change the growth rate of the instabilities. However, the structures developed as a result of sequential multiwavelengths are independent of the absolute growth rate of the instabilities and the final results will remain unchanged.

Case VI: two unstable sources covered by a denser overburden

By means of linear stability analysis Ramberg (1973) showed the possibility of simultaneous development of diapirs with two wavelengths in models having two unstable source layers, where the lower source was less dense than the upper source (case VI, Fig. 2). The

density stratification of case VI, with its two density inversions, has two potential overturns, one for each active interface. Polydiapirs may develop if the two potential overturns have different wavelengths. Numerical models with systematic variations in the physical and geometrical parameters were calculated to define the conditions necessary for the development of such polydiapirs. Ramberg (1973) modelled an overburden of an infinite half space, but finite thicknesses are modelled here. Jackson et al. (1990) modelled analytically a case VI density stratification using finite overburden. Their results showed the development of a single wavelength in layer sequences with the same viscosity ($m = 1$) but different thickness relations.

Viscosity ratio variations

A series of models were calculated for case VI (Fig. 2), where thicknesses and densities were kept constant and only the viscosity ratio (m), between overburden (layer 1) and source (layers 2 and 3) was varied (Fig. 5). The results of the calculations (Figs. 5a–d) show that when m is increased, the overturn of the unstable sequence changes from single wavelength diapirs ($m = 50$), to simultaneous polydiapirs ($m = 100$ and 200), to sequential polydiapirs ($m = 500$).

When $m = 50$ (Fig. 5a), the overturn is dominated by the growth of perturbations at the top interface 1, and only single wavelength diapirs are obvious. Due to the low density contrasts between layers 2 and 3, and their relatively high viscosity as compared to the overburden layer 1, the potential short wavelength instabilities at interface 2 grow too slowly to be able to develop significant amplitudes.

As the value of m increases, the source layers become more mobile relative to the overburden. This increases the growth rate of perturbations at interface 2. When $m = 100$ and 200 (Figs. 5b & c), the short wavelength diapirs at interface 2 develop only slightly faster than the longer wavelength diapirs at interface 1. The result is the development of a 'simultaneous' multiwavelength overturn. For values of $m = 500$ (Fig. 5d), perturbations at interface 2 develop much faster than those at interface 1, which acts as an almost rigid boundary. Perturbations at interface 1 begin to be noticeable only when the small-scale diapirs at interface 2 are already mature, and the overturn between layers 2 and 3 is advanced. The perturbations at interface 1 grow with a long wavelength and the small diapirs merge to form the large, widely spaced diapirs required by the overturn at interface 1. In Fig. 5(d) ($m = 500$) the short wavelength diapir growing at the centre of the box was later flattened and laterally stretched in the syncline between two large-scale diapirs. The final result is an amoeboid mass of layer 3 fluid at the top of the large diapirs; thin stems of the early small-scale diapirs are still visible. In natural examples extremely detailed mapping would be needed in order to recognize the polydiapiric evolution of the structure, thus the final pattern could be incorrectly interpreted as
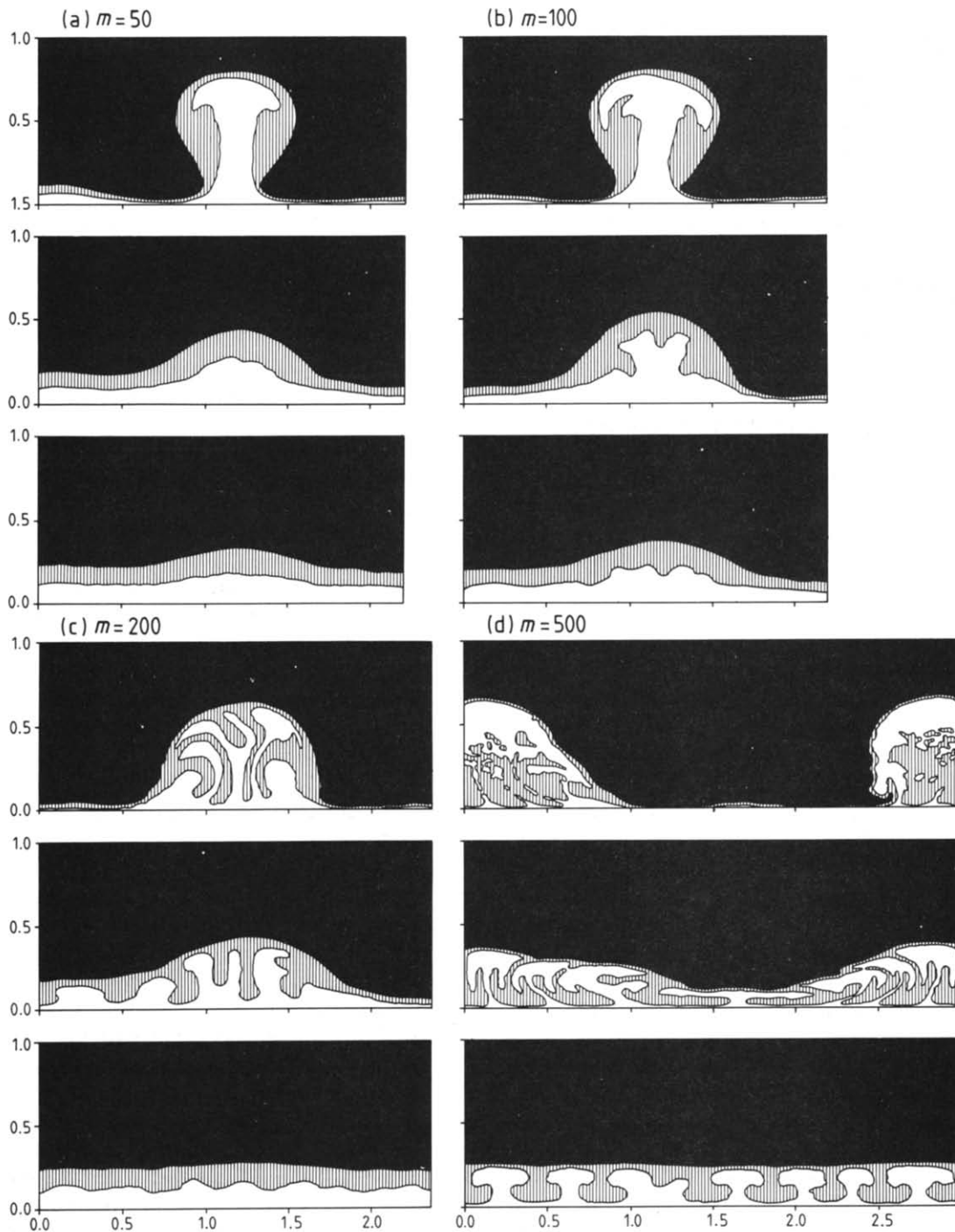
Fig. 5. Results of model calculations for case VI where non-dimensional densities are $\rho_1 = 1.0$, $\rho_2 = 0.9$ and $\rho_3 = 0.89$, $\Delta\rho_1\Delta\rho_2 = 10$; the combined thickness of the source layers (h_s) is 0.25 (scaled by the height of the box) and where m is the variable viscosity ratio between layers 1 and 2–3. The size of the box was varied in accordance with the estimated size of the characteristic wavelength of the long wave.

a simple overturn of a two layer source. For even higher viscosity ratios, overturn between the two source layers may be expected to be complete prior to the rise into layer 1. The sequence evolves from case VI density stratification towards case V (Fig. 2), but it is possible that no evidence of this process will survive into the late stages of evolution. For cases of sequential multiwavelength the problem simplifies to the two-layer system, as discussed earlier, where no slip occurs at either the top or bottom.

Density variations

In contrast to case IV, density variations strongly affect the structural development of case VI density stratifications. The density difference ratio, $\Delta\rho_1/\Delta\rho_2 = (\rho_1 - \rho_2)/(\rho_2 - \rho_3)$, defines the relative density difference across the internal interfaces of the model. This parameter is more important than the density difference across a single interface in controlling the development of polydiapiric structures. For a given set of viscosities
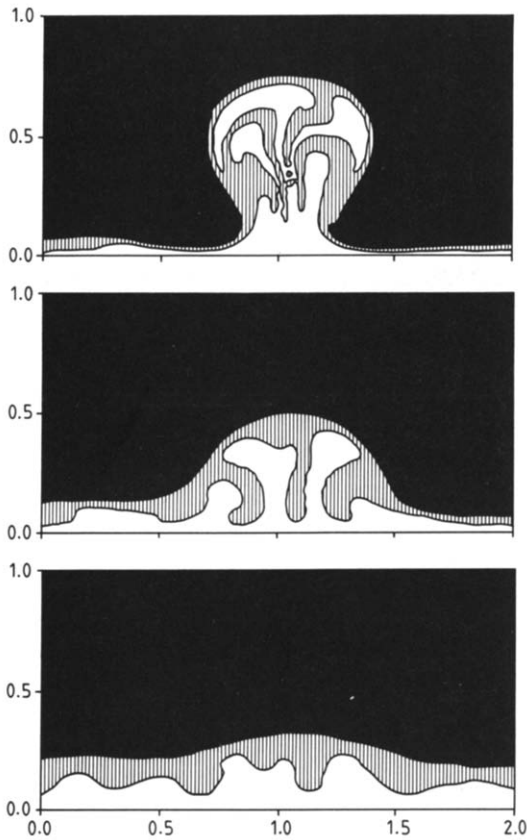
Fig. 6. Results of model calculations for case VI where $\Delta\rho_1/\Delta\rho_2 = 3.3$ and $m = 50$.

Fig. 7. Log plot of $(\Delta\rho_1/\Delta\rho_2) \times m$ for calculation of case VI where combined thickness of the source layers (h_s) was kept constant and equal to 0.25 of the box height.

and layer thicknesses, the density difference across an interface controls the growth rate of the instabilities at that interface. The density difference ratio is thus an indirect measure of the growth rate ratio of the instabilities at the two interfaces.

The calculations described in the previous section had a density difference ratio $(\Delta\rho_1/\Delta\rho_2)$ of 10. Even for such small values of $\Delta\rho_2$ in relation to $\Delta\rho_1$, short wavelength diapirs at interface 2 were able to develop for a viscosity contrast of as low as 100. A series of calculations were made where the density difference between the source layers, $\Delta\rho_2 = \rho_2 - \rho_3$, was increased to 0.03, and $\Delta\rho_1/\Delta\rho_2$ assumed a value of 3.3. An increase in the density difference between the two source layers enhances the growth rate of the smaller diapir at interface 2. The lowest limit of m can therefore be decreased and polydiapirs will still develop. The results show that for $m = 50$ (Fig. 6), the polydiapirs developed are similar to those obtained for $m = 200$ when $\Delta\rho_1/\Delta\rho_2 = 10$ (Fig. 5c). The inverse occurs when the density difference ratio is increased. The limiting value of m tends towards infinity as the density difference between the source layers tends to zero ($\Delta\rho_1/\Delta\rho_2$ tends to infinity).

The values of m and $\Delta\rho_1/\Delta\rho_2$ limiting the formation of case VI polydiapirs for source thickness (h_s) 0.25 are summarized in Fig. 7. The boundary of the fields of single wavelength diapirs and polydiapirs is expressed by the equation

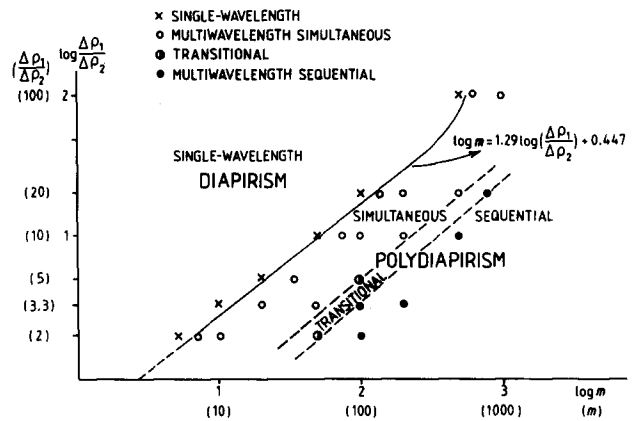$$\log m = 1.29 \log (\Delta\rho_1/\Delta\rho_2) + 0.447. \qquad (15)$$

Where the value of $\Delta\rho_1/\Delta\rho_2$ is zero the driving force at the upper interface disappears, and the equation is no longer valid. Figure 7 also shows the limit between the field where polydiapirs develop simultaneously and sequentially. The boundary between these behaviours is transitional but follows roughly the same slope as the well-defined boundary defined by equation (15).

Thickness variations

The influence of thickness variations on the development of the structures in the two-source-layer model is complex. The manner in which the polydiapirs develop depends on how the thickness variations affect the characteristic wavelength (λ_c) and its growth rate for each specific interface. The influence of thickness ratios on systems with a single source covered by a single overburden is well known (Woidt 1980, Ramberg 1981, Rönnlund 1989). Rönnlund (1989) showed that for a two-layer system with free-slip at the top and no-slip at the bottom, an increase in the thickness of the source layer causes an increase of the λ_c, that reaches a maximum when layers have equal thicknesses. A further increase in the source thickness causes a decrease in λ_c. Ramberg (1981) developed a mathematical solution for multilayered systems where the interaction between several source layers can be studied for infinitesimal amplitudes of the instabilities. A similar mathematical approach was used by Jackson et al. (1990) in order to explore the influence of thickness variations on a two-source sequence.

A series of calculations were made where only the total thickness of the source (h_s) was changed, not the relative thickness between the two source layers (which were maintained at equal thickness). The model parameters and results of the calculations are shown in Fig. 8. For h_s less than 0.4 the instabilities at interface 2 were dominated by the fast-growing long wavelength at interface 1. Polydiapiric structures developed for h_s values of 0.5, whereas a single wavelength developed for $h_s = 0.6$ or larger. For these high values of h_s, polydiapiric structures did not develop because the λ_c for interfaces 1
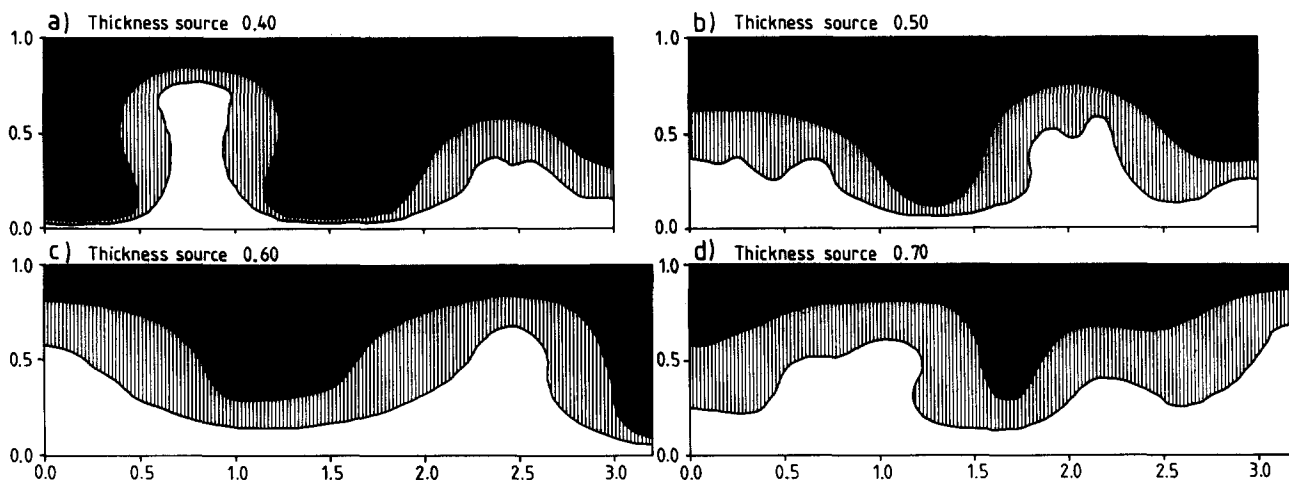
Fig. 8. Results for different thicknesses of the whole source when the other parameters are kept constant (case VI).

and 2 are sufficiently close (from graphs in Rönnlund 1989) for both interfaces to overturn with a common wavelength.

Three-dimensional physical model

Natural diapiric provinces generally involve three-dimensional variations that modify the simple two-dimensional structures modelled here. A physical model was built to observe the three-dimensional development of polydiapiric structures in an example of a case VI density stratification.

Physical models of gravitationally unstable sequences have previously been studied, among many others, by Nettleton (1943), Ramberg (1963, 1981), Dixon (1975), Whitehead & Luther (1975), Talbot (1977), Jackson & Talbot (1989a) and Koyi (1990). The model developed here was built in a cylindrical container of transparent Plexiglas. The transparent Newtonian polydimethyl-siloxane (PDMS described in Weijermars 1986) was used for the overburden. Hyvis 150, an artificial poly-butene oil produced by B.P. Chemicals, was used to build the two source layers. The lower source layer was of pure Hyvis 150, whereas the upper source was mixed, to a translucent long lived suspension, with fine-grained barite ($BaSO_4$) to increase the bulk density. Tests have shown that the addition of small amounts (e.g. <10%) of barite to Hyvis does not affect its viscosity significantly. The geometrical parameters of the model and the physical properties of the material layers are shown in Fig. 9(a). The model is dynamically analogous to a Newtonian natural sedimentary sequence with the same geometrical proportions and density ratios (Weijermars & Schmeling 1986).

The unstable sequence was allowed to develop under normal gravity, and without any imposed perturbations other than those inherent in building the model. The results are shown in Figs. 9(b)–(f). The initial random perturbations at interface 2 between the two source layers developed rapidly into ring-shaped short-wave diapiric and anti-diapiric (downwards directed) walls parallel to and controlled by the rigid lateral boundaries

(Fig. 9b). As in the numerical models, the early overturn of the unstable layers is confined to the two mobile source layers and interface 1 acts as a stiff boundary during the 'incubation period' (Biot & Odé 1965). However, in contrast to the two-dimensional numerical models, the ring-shaped walls already have three-dimensional irregularities at this stage and these will be enhanced with time. The next step was the growth of a long wavelength dome at interface 1 (Figs. 9c & d). This growth caused a large-scale flow throughout the model, leading to incorporation within the large-scale dome of the short wavelength diapirs that had developed earlier. At this stage the internal ring walls show individual finger diapirs and anti-diapirs.

The final structure shown in Figs. 9(e) & (f) is qualitatively very similar in vertical cross-section to the polydiapiric structures calculated in the numerical models (e.g. Figs. 5b–d). A horizontal section through the upper part of the model shows a simple diapir formed by model material 3. A section through a lower part of the model (Fig. 9e) shows a complex structure where the lower layer 3 occurs in the internal and external parts of the diapir, whereas lobes and cusps in the sinking layer 2 simulate vertical plunging curtain folds.

The polydiapiric structures in the physical and numerical models are similar. Rather than being due solely to the convergent flow into the diapiric stem (Ramberg 1963), the formation of curtain folds in this model is related to initial three-dimensional heterogeneities that caused the ring walls to develop into several short wavelength diapirs. Lobes and cusps correspond to regions dividing the small diapirs.

IMPLICATIONS OF THE MODELS TO NATURE

Whilst a few granitic terrains have been interpreted as polydiapirs (e.g. Stephansson 1975, Schwerdtner 1982, Collins 1989), polydiapiric structures have never previously been explicitly suggested for the well known salt domes; although such structures have appeared in illustrations of these (Fig. 11). This study shows that polydia-
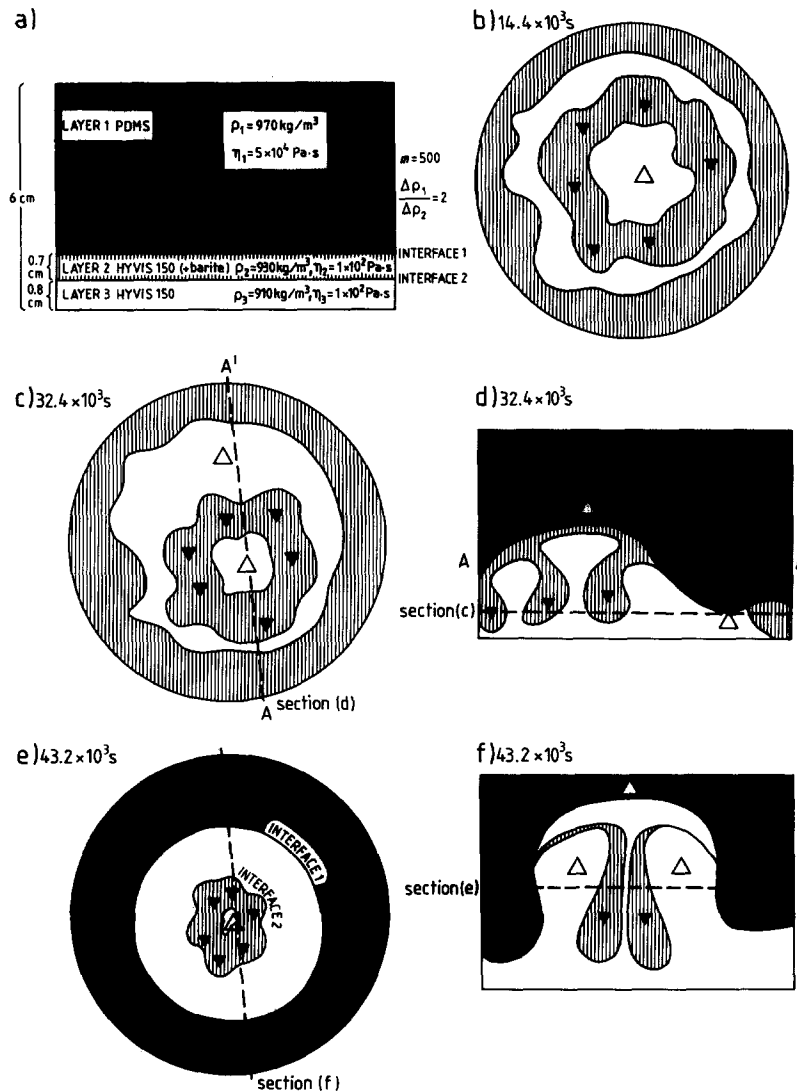
Fig. 9. (a) Parameters and initial geometry of the physical model. (b)–(f) Vertical and horizontal sections of different stages of development of the overturn are traced from photographs. The small black downward-pointing triangles correspond to the positions of short wavelength anti-diapirs, and the large white upward-pointing triangles correspond to the position of the large diapir and anti-diapir.

pirs may be common in both types of rock sequences, and that several of the structures common within salt domes may result from this complex type of diapirism.

A remarkable feature of the results presented in Fig. 5 is that polydiapirs are likely to develop for reasonable viscosity contrasts between salt layers and overlying clastic rocks ($m > 50$), at very low density differences between the two salt layers (1%). Such very small density differences are likely in natural evaporitic sequences, and salt layers previously modelled as a single homogeneous source may in fact behave as a multi-layered source and overturn internally, leading to poly-diapiric structures (case VI). The experimental results show that very small variations in densities and viscosities can lead to very different structures since case VI polydiapirs are a result of the interaction and competition of the two characteristic wavelengths. Significant changes in the structures developed during overturn may occur if the materials have yield strengths and/or non-Newtonian behaviour. In contrast to case VI, case IV polydiapirs are unlikely to be very different for non-

Newtonian materials, provided that the λ_c and growth rates of the two phases of overturn differ significantly.

Extrapolating the results of two-dimensional calculations for perfectly homogeneous materials to three-dimensional heterogeneous sedimentary rocks, suggests that large differences in the behaviour of the overturns may be expected in different parts of the same sedimentary basin. Polydiapirs may develop in some areas whereas single wavelength diapirs could develop in others.

The sequence of sediments in northern Germany is formed by a lower buoyant layer of pure salt, 600 m thick (Na 2 of Richter-Bernburg 1955), covered by an impure, equally thick layer of mixed evaporitic and argillaceous rocks (Z3 and Z4). These layers are covered by a more viscous clastic overburden. The salt diapirs developed in this area are characterized by internal, cylindrical, steeply plunging folds known as curtain folds (Kulissen-falten; Richter-Bernburg 1955, fig. 16). Curtain folds have been attributed to buckling of competent layers embedded in incompetent buoyant rock that undergoes
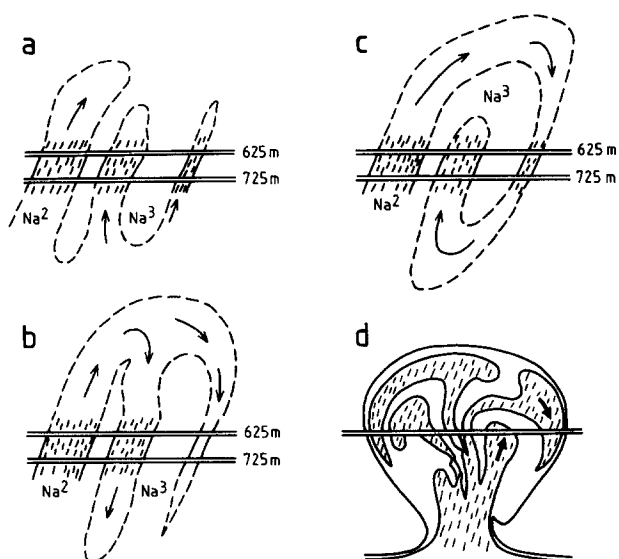
Fig. 10. (a) & (b) Upward-facing folds and rolling folds, after Richter-Bernburg (1980); (c) vortex, after Talbot & Jackson (1987); and (d) upward and rolling folds resulting from polydiapirs (from Fig. 6).

convergent flow towards and up the stem of diapirs (Ramberg 1963, 1981). The result of the physical model (Fig. 9) shows that curtain folds can also develop as a result of polydiapirism.

Masses of salt known as spines that have moved in different directions or at different rates are separated by shear zones in salt diapirs along the coast of the Gulf of Mexico (e.g. Kupfer 1976). The present study confirms the suggestion by Talbot & Jackson (1987) that spines within diapirs could be a result of small scale diapirs within a large diapir.

Repetition of the same salt layer is a common feature within natural salt diapirs. Richter-Bernburg (1980) questioned whether such a repetition was caused by simple upward-facing folds or by 'rolling folds', where anticlines of salt were transformed into synclines (Figs. 10a & b). Talbot & Jackson (1987) suggested that internal circulation inside the rising diapir could cause layer repetition by 'vortex type rolling folds' (Fig. 10c). The numerical models presented here add another possible alternative. Polydiapirs can also lead to a repetition of salt layers both by upward-facing folds and by downward-facing rolling folds (Fig. 10d).

Hofrichter (1967) and Richter-Bernburg (1980) present schematic block-diagrams of the Stade and the Benthe salt diapirs where several internal small diapirs develop inside the main ones (Figs. 11a & b). The close resemblance between their diagrams and some of the results obtained here (Fig. 11c) is alone sufficient justification for the suggestion that polydiapirism in nature may be far more important than previously recognized.

CONCLUSIONS

Polydiapiric evolution of gravitation instabilities is an alternative explanation for the origin of several well known structures in salt diapirs.
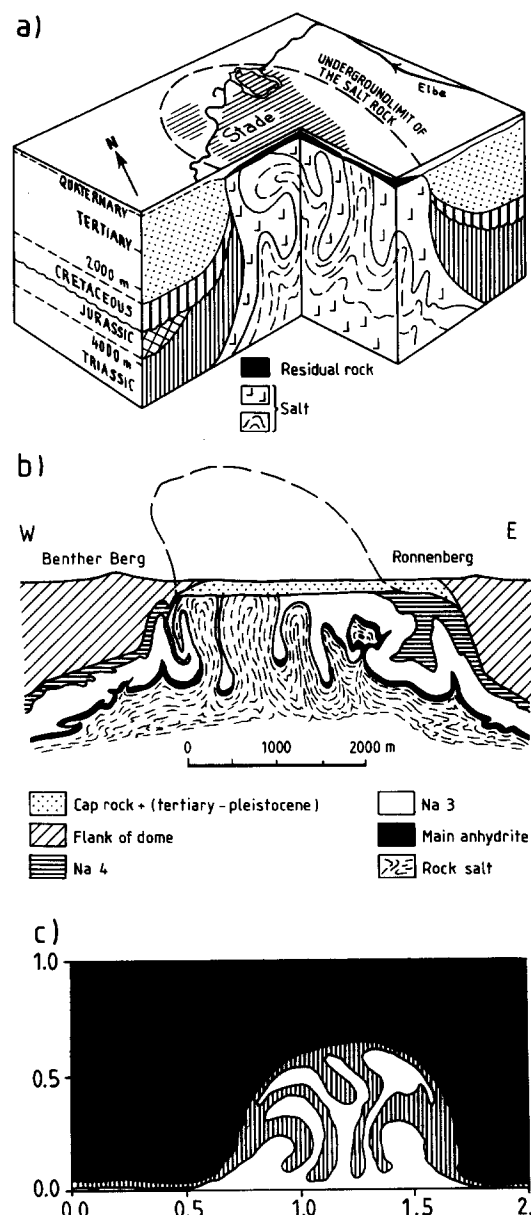

Fig. 11. (a) The Stade salt diapir (after Hofrichter 1967); and (b) the Benthe diapir (after Richter-Bernburg 1980); (c) result obtained in Fig. 5(c) shown for comparison.

Calculations show that polydiapirism, can be sequential or simultaneous in two geologically important triple-layered stratifications. The density stratification of case IV (Fig. 2) only develops sequential multiwavelength when the upper overburden is significantly stiffer than the two underlying layers. Sequential polydiapirism is characterized by an overturn between the two lower layers before the later overturn between the source layer and the upper stiff overburden. This stratification simulates a dense anhydrite layer overlying buoyant halite beneath stiff clastic sedimentary rocks. The density stratifications of case VI (Fig. 2) may develop both simultaneous or sequential multiwavelengths. Very small density decreases in the source layer may lead to polydiapirism. This fact suggests that natural layers previously modelled as a single homogeneous stratum may behave as multilayers during diapirism, and lead to polydiapiric structures.

Sequential polydiapirism develops because two source layers overturn before the source and overburden start to overturn. The result can be large diapirs in which no structural evidence of the first overturn remains.

The patterns resulting from the different models described here depend on the interaction and competition between the two potential wavelengths of the two interfaces. Thus, thickness, viscosity and density ratios play major roles because they control the wavelength and growth rate of the two sets of instabilities.

The main conclusion of this study is that any work carried out in structures in gravitationally unstable rock sequences should take into account the possibility of polydiapirism.

REFERENCES

Boit, M. A. & Odé, H. 1965. Theory of gravity instability with variable overburden and compaction. *Geophysics* **30**, 213–227.

Collins, W. J. 1989. Polydiapirism of the Archaean Mount Edgar batholith, Pilbara block, Western Australia. *Precambrian Res.* **43**, 41–62.

Dixon, J. M. 1975. Finite strain and progressive deformation in models of diapiric structures. *Tectonophysics* **28**, 89–124.

Hofrichter, E. 1967. Subrosion und Bodensenkungen am Salzstock von Stade. *Geol. Jb.* **84**, 327–340.

Jackson, M. P. A., Cornelius, R. R., Craig, C. H., Gansser, A., Stöcklin, J. & Talbot, C. J. 1990. Salt diapirs of the Great Kavir, Central Iran. *Mem. geol. Soc. Am.* **177**.

Jackson, M. P. A. & Talbot, C. J. 1986. External shapes, strain rates, and dynamics of salt structures. *Bull. geol Soc, Am.* **97**, 305–323.

Jackson, M. P. A., Talbot, C. J. & Cornelius, R. R. 1988. Centrifuge modeling of the effects of aggradation and progradation on syn-depositional salt structures. *Univ. Texas at Austin, Bur. Econ. Geol. Rep. Invest.* **173**.

Jackson, M. P. A. & Talbot, C. J. 1989a. Salt canopies. *Gulf Coast Sec. Soc. Econ. Paleont. Miner. Fdn. 10th Annual Res. Conf. Prog. Extd. & Illus. Abs.*, 72–78.

Jackson, M. P. A. & Talbot, C. J. 1989b. Anatomy of mushroom-shaped diapirs. *J. Struct. Geol.* **11**, 211–230.

Jenyon, M. K. 1986. *Salt Tectonics*. Elsevier, London.

Koyi, H. 1990. Reactivation; another mechanism for the formation of mushroom diapirs. *Geol. Soc. Am. Abs. w. Prog.* **22**, 7.

Kupfer, D. H. 1976. Shear zones inside the Gulf Coast salt stocks help to delineate spines of movement. *Bull. Am. Ass. Petrol, Geol.* **60**, 1434–1447.

Nettleton, L. L. 1943. Recent experimental and geophysical evidence of mechanisms of salt-dome formation. *Bull. Am. Ass. Petrol. Geol.* **27**, 51–63.

Ramberg, H. 1963. Experimental study of gravity tectonics by means of centrifuged models. *Bull. geol. Instn. Univ. Uppsala* **XLII**.

Ramberg, H. 1968. Fluid dynamics of layered systems in the field of gravity, a theoretical basis for certain global structures and isostatic adjustment. *Phys. Earth & Planet. Interiors* **1**, 63–87.

Ramberg, H. 1973. Model studies of gravity-controlled tectonics by the centrifuge technique. In: *Gravity and Tectonics* (edited by Dejong, K. A. & Scholten, R.). New York, John Wiley & Sons, 49–69.

Ramberg, H. 1981. *Gravity, Deformation and the Earth's Crust in Theory, Experiments and Geological Application* (2nd edn.). Academic Press, London.

Richter-Bernburg, G. 1955. Stratigraphische Gliederung des deutschen Zechsteins. *Z. dt. geol. Ges.* **105**, 843–854.

Richter-Bernburg, G. 1980. Salt tectonics: interior structures of salt bodies. *Bull. Cent. Rech. Explor.-Prod. Elf-Aquitaine* **4**, 373–393.

Rönnlund, P. 1989. Viscosity ratio estimates from natural Rayleigh–Taylor instabilities. *Terra Nova* **1**, 344–348.

Schmeling, H. 1987. On the relation between initial conditions and late stages of Rayleigh–Taylor instabilities. *Tectonophysics* **133**, 65–80.

Schwerdtner, W. M. 1982. Salt stocks as natural analogues of Archaean gneiss diapirs. *Geol. Rdsch.* **71**, 370–379.

Schwerdtner, W. M. & Osadetz, K. 1983. Evaporite in the Sverdrup basin: new insight and unsolved problems. *Bull. Can. Petrol. Geol.* **31**, 27–36.

Stephansson, O. 1975. Polydiapirism of granitic rocks in the Svecofennian of central Sweden. *Precambrian Res.* **2**, 189–214.

Talbot, C. J, 1977. Inclined and asymmetrical upward-moving gravity structures. *Tectonophysics* **42**, 159–181.

Talbot, C. J. & Jackson, M. P. A. 1987. Internal kinematics of salt diapirs. *Bull. Am. Ass. Petrol. Geol.* **71**, 1068–1093.

Urai, J. L., Spiers, C. J., Zwart, H. J. & Lister, G. S. 1986. Weakening of rock salt by water during long term creep. *Nature* **324**, 554–557.

Weijermars, R. 1986. Flow behaviour and physical chemistry of bouncing putties and related polymers in view of tectonic laboratory applications. *Tectonophysics* **124**, 325–358.

Weijermars. R. & Schmeling, H. 1986. Scaling of Newtonian and non-Newtonian fluid dynamics without inertia for quantitative modelling of rock flow due to gravity (including the concept of rheological similarity). *Phys. Earth & Planet. Interiors* **43**, 316–330.

Whitehead, J. A., Jr & Luther, D. S. 1975. Dynamics of laboratory diapir and plume models. *J. geophys. Res.* **80**, 705–717.

Woidt, W. D. 1978. Finite element calculations applied to salt dome analysis. *Tectonophysics* **50**, 369–386.

Woidt, W. D. 1980. Analytische und numerische modellexperimente zur physik der salzstockbildung. Unpublished dissertation, Technische Universitat, Braunschweig.